Pop-in events induced by spherical indentation in compound semiconductors

J.E. Bradby[a)] and J.S. Williams
Department of Electronic Materials Engineering, Research School of Physical Sciences and Engineering, The Australian National University, Canberra, ACT 0200, Australia

M.V. Swain[b)]
Biomaterials Science Research Unit, Department of Mechanical and Mechatronic Engineering, and Faculty of Dentistry, The University of Sydney, Eveleigh, NSW 1430, Australia

(Received 16 June 2003; accepted 31 October 2003)

Details of the elastic–plastic transitions in crystalline compound semiconductors have been examined using spherical indentation. Two cubic (InP and GaAs) and two hexagonally structured semiconductors (ZnO and GaN) have been studied. A series of indentations have been made in each material at a number of different loads. The resulting load–penetration curves exhibited one or more discontinuities on loading (so called pop-in events). The load at which the initial pop-in event occurred has been measured along with the corresponding indenter extension. The elastic and elastic–plastic response of each material to spherical indentation has been calculated and compared with the experiment. By taking the difference between the elastic and elastic–plastic penetration depths, it has been found that the pop-in extension at each load could be predicted for each material. The detailed deformation behavior of each of the materials during indentation has also been discussed.

I. INTRODUCTION

It is now widely recognized that features in nanoindentation load–penetration curves can provide valuable insights into the response of materials during deformation.[1–8] For example, prominent features in the load–penetration curve can be associated with microstructural events including cracking, film delamination, and the generation and propagation of dislocations.[1–9]

On nanoindentation loading, a discontinuity in the measured depth is commonly referred to as a pop-in event with a similar discontinuity on unloading called a pop-out event. The pop-in event usually represents the sudden yielding of a material under load. It is routinely observed in samples with a crystalline structure and has widely been associated with the onset of plasticity.[1–8] Previous indentation studies have observed a pop-in event in the loading curves taken from the compound semiconductors GaAs, InP, GaN, and ZnO.[8,10–19] It has been shown that the mode of deformation in these compound semiconductors[10–12] does not involve a phase transformation, as has been previously observed in Si.[20] Unlike Si, no discontinuities have been reported in the unloading curves (pop-out events) from these compound semiconductors at room temperature.[10,18,19] Previous transmission electron microscopy (TEM) studies of GaAs,[10,21–23] InP,[10,18,19,22,24] GaN,[11,25] and ZnO[12] after indentation have shown that these materials deform by the generation and propagation of dislocations. No evidence has been observed that oxide cracking contributes to the pop-in event. Such indentation studies have also shown that the onset of plasticity in GaAs, InP, and ZnO appears to be a far more catastrophic event than for GaN. Indeed, the average contact pressure before the pop-in event has been observed to increase to more than twice the accepted hardness[26] value in GaAs, InP and ZnO before abruptly falling to remain at a relatively constant level with increasing indenter penetration.[10,15–17] [Note that throughout this paper, we shall refer to the "average contact pressure" before the pop-in event (in the elastic regime) and "hardness" after the pop-in event. For details on definitions of hardness, see Ref. 26.]

Although many deformation studies involving nanoindentation are routinely conducted using pointed indenters (Vickers or Berkovich), the use of spherical indenters can be advantageous. It has been shown that, compared with pointed indenters, spherical indenters produce a more uniform resultant stress field and provide an extended elastic–plastic regime before cracking is initiated. In addition, and important to this current study, it is possible

[a] Address all correspondence to this author.
e-mail: Jodie.Bradby@anu.edu.au
[b)] This author was an editor of this focus issue during the review and decision stage. For the *JMR* policy on review and publication of manuscripts authored by editors, please refer to http://www.mrs.org/publications/jmr/policy.html

 © 2004 Materials Research Society

to analytically calculate both the elastic and elastic–plastic response of materials to spherical indentation. Although this is well documented in the literature, we will briefly present the relations needed to calculate this behavior. The elastic response of a material to spherical indentation loading can easily be determined if the elastic properties of both the indenter and the sample are known.[27] The classical relationship giving the elastic depth of penetration by a sphere is given in Eq. (1):

$$\delta = \left(\frac{9}{8}\right)^{1/3}\left(\frac{1}{E^*}\right)^{2/3}\left(\frac{1}{D}\right)^{1/3} P^{2/3} \quad , \tag{1}$$

where δ is the depth of penetration of the indenter, $D = 2R$ where R is the radius of the spherical indenter, and P is the applied load. E^* is the compound modulus given by Eq. (2):

$$\frac{1}{E^*} = \frac{(1-\nu_s^2)}{E_s} + \frac{(1-\nu_i^2)}{E_i} \quad , \tag{2}$$

where E_s and ν_s are the modulus and Poisson ratio of the sample, respectively, and E_i, and ν_i are the modulus and Poisson ratio of the diamond indenter (1100 GPa and 0.1), respectively.[28]

The elastic–plastic response of a material to spherical indentation can also be analytically calculated using the model of Field and Swain. This method is well-described elsewhere[28,29] and therefore will only be outlined in brief here. The Field and Swain technique uses the finding of Sneddon[30] that the elastic displacement (δ) of a surface by a spherical indenter above and below the circle of indenter contact are equal for purely elastic loading. The depth of penetration below the circle of contact between the indenter and the sample h_p can be calculated using a step-wise unloading process (load–partial unload) where the ratio of the final depth and the partially unloaded depth are measured. From this loading–unloading process, h_p can be calculated using Eq. (3):

$$h_p = \left(\frac{h_t + h_r}{2}\right) \quad , \tag{3}$$

where h_t is the total depth and h_r is the residual depth. The hardness and modulus are then determined using h_p together with a detailed knowledge of the radius of the indenter tip.

Finally, for this current study, it is especially important to define the point at which a material exhibits plasticity. The onset of full plastic flow is defined by the Field and Swain technique using the well-known relation shown in Eq. (4):

$$\left(\frac{p_m}{Y}\right) = 3 \quad , \tag{4}$$

where p_m is the average pressure over the circle of contact and Y is equal to the yield stress. After the pop-in event, p_m is equivalent to the hardness of the material, and thus the elastic–plastic behavior depends critically on this value. The critical load (P_c) corresponding to the onset of plastic flow (with no work hardening) is given by Eq. (5):

$$P_c = \left(\frac{9}{16}\right)\left(\frac{R}{E^*}\right)^2 (3\pi Y)^3 \quad . \tag{5}$$

Thus, above P_c the indenter depth can be calculated using the method of Field and Swain.[28] The unloading behavior can also be modeled assuming an elastic recovery.

II. EXPERIMENTAL

In this study, spherical indentation was used to induce pop-in events in four compound semiconductor materials, the details of which are shown in Table I. Note that two materials had a cubic structure and the others a hexagonal structure. The indents were made on the (100) surface in GaAs and InP and the (0001) face in ZnO and GaN. GaAs, InP, and ZnO were bulk samples whereas GaN consisted of an approximately 2-μm epilayer grown on a sapphire substrate. Each material was indented using an ultra-micro indentation system (UMIS 2000) (Commonwealth Science and Industrial Research Organization, Sydney, Australia) at room temperature and at ambient pressure. A continuous load–unload cycle was employed with a spherical indenter of approximately 4.2-μm radius. The radius of the indenter was carefully calibrated by loading in fused silica of known mechanical properties and by imaging in a scanning electron microscope.

Using the measured mechanical properties given in Table I, the theoretical elastic response of each of the materials was calculated using Eq. (1) for loads up to 50 mN using a sphere of approximately 4.2-μm radius. The theoretical elastic–plastic behavior was also calculated using the Field and Swain technique[28] and the measured values shown in Table I.

III. RESULTS AND DISCUSSION

A typical load–penetration curve measured by loading GaAs to 50 mN is shown in Fig. 1(a). This plot shows a

TABLE I. The compound semiconductors studied here showing their respective crystal structure, hardness and modulus. The hardness values shown here were directly measured after the pop-in event before any effects of work hardening or cracking were observed, and the modulus values are the measured compound moduli.

Material	Structure	Hardness (GPa)	Modulus (GPa)
GaAs	Cubic	6.5	98
InP	Cubic	3.9	83
ZnO	Hexagonal	3.6	111
Epilayer-GaN	Hexagonal	12.5	233

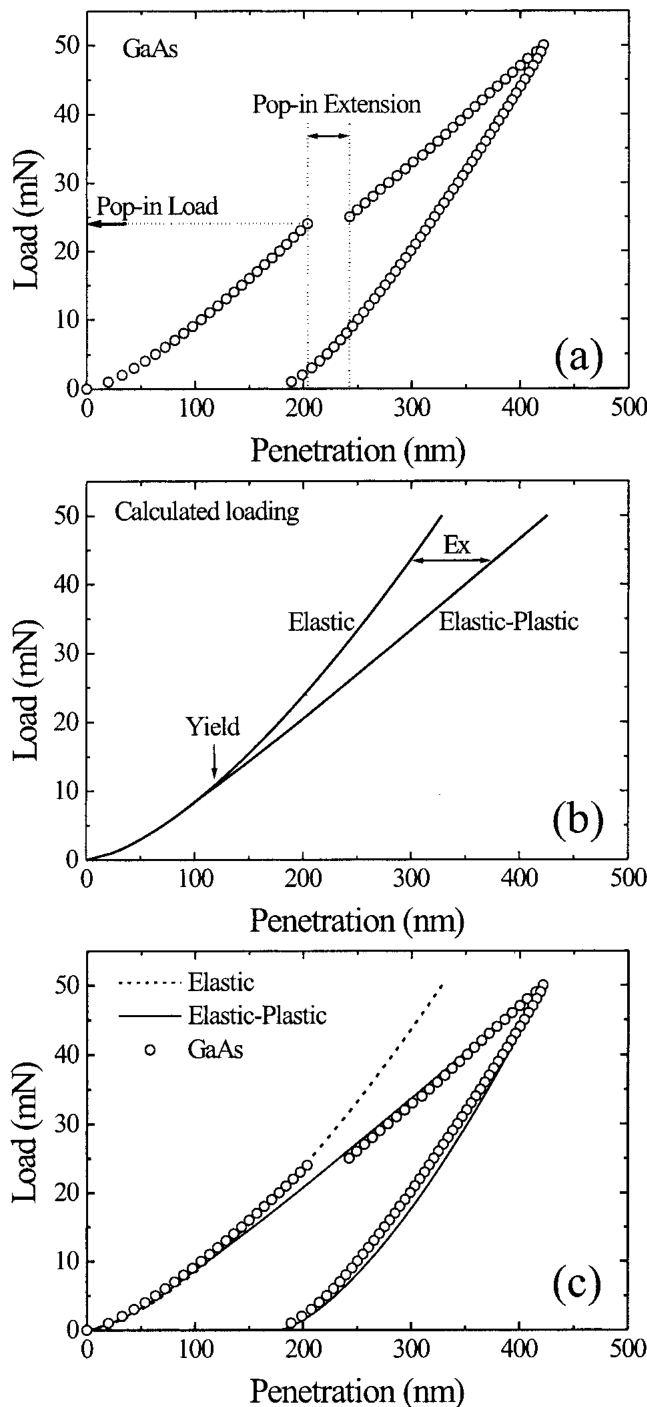

FIG. 1. (a) Load–penetration curve for GaAs loaded to 50 mN showing the pop-in load and the pop-in extension. (b) Calculated load and maximum indenter penetration values for GaAs. The elastic curve was calculated using an elastic contact relationship[27] and elastic–plastic data was calculated using the Field and Swain method.[28] (c) Both the experimental and calculated curves for GaAs.

prominent discontinuity during loading (pop-in event) at approximately 24 mN. At pop-in, the indenter undergoes a sudden extension of approximately 38 nm. The load at which the pop-in event was observed to occur for GaAs was found to vary between 23 and 45 mN.[10]

Figure 1(b) shows the calculated elastic and elastic–plastic responses of GaAs loaded to 50 mN. The two curves are identical up to the the yield point [P_c in Eq. (5)], which occurs at a load of about 9 mN. After yield, there is a notable difference in the calculated indenter penetration for the elastic and elastic–plastic responses. For example, at a load of 40 mN the calculated elastic depth of penetration is approximately 280 nm and the elastic–plastic penetration is approximately 350 nm; a difference of about 70 nm. The difference between these two curves is labeled as Ex in Fig. 1(b) and will be used later in this paper.

Figure 1(c) shows both the experimental and calculated (elastic and elastic–plastic) load–penetration curves for GaAs. It is interesting to note that the load at which the pop-in event occurs (~24 mN) is higher than the yield point predicted from Eq. (5) (~9 mN). We will comment further on this effect later in the paper. Below the pop-in event (<24 mN), the measured data is observed to follow the calculated elastic response. After pop-in, the measured data now overlaps the calculated elastic–plastic curve. This implies that the difference in the depth of penetration between the calculated elastic and calculated elastic–plastic responses should give the pop-in extension as defined in Fig. 1(a). Thus, we can use these calculated loading behaviors to predict the extent of the pop-in event at each load in each material.

The pop-in load and extensions [as defined in Fig. 1(a)] were measured in a number of individual load–penetration curves for each of the materials studied. A plot showing the load at pop-in as a function of the extension at pop-in is shown for GaAs and InP in Fig. 2(a) and for ZnO and GaN in Fig. 2(b). In addition to the experimentally measured data, these plots also show the calculated relationship between pop-in load and indenter extension for each material. The calculated pop-in data was determined by taking the difference between the predicted indenter depths for the elastic and elastic–plastic responses [Ex in Fig. 1(b)]. Note that the calculated data were generated purely using the mechanical properties of the materials given in Table I and the properties of the spherical diamond indenter. No fitting parameter was used. The properties listed in this table were measured using the UMIS and have been reported elsewhere.[10,16,17] As can be seen in Fig. 2, the calculated data appears to agree broadly with the measured pop-in extensions at each load.

It is interesting to note that the harder materials, GaAs and GaN, both display larger gradients (pop-in load/pop-in extension) in Fig. 2 than the softer semiconductors of InP and ZnO. Indeed, it was found that this gradient scales with the hardness as shown in Fig. 3. The smallest gradient value (0.17 mN/nm) corresponds to the material with the smallest hardness value (3.6 GPa for ZnO) and the highest gradient value (0.84 mN/nm) corresponds to

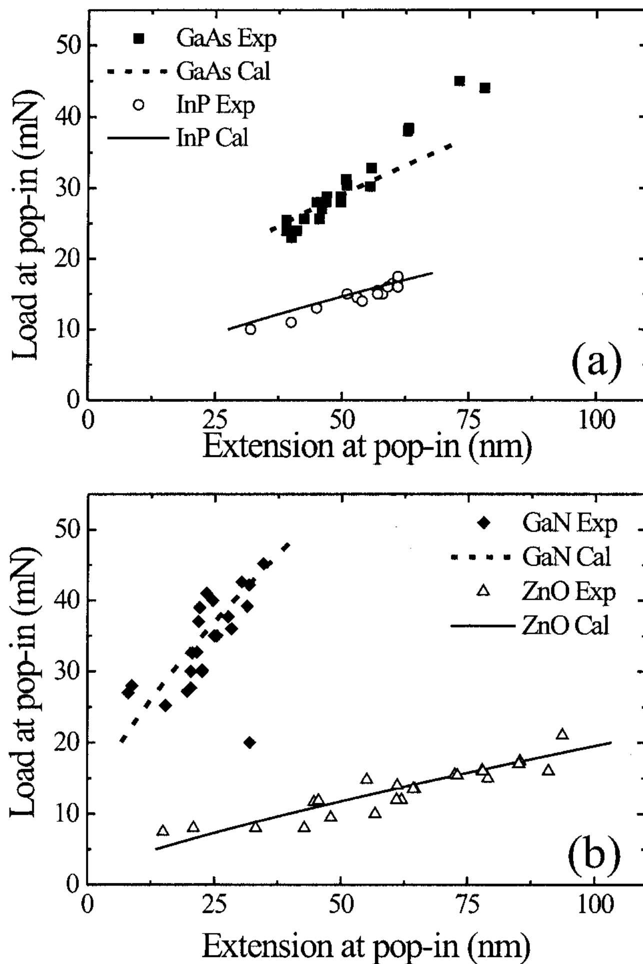

FIG. 2. Experimental (Exp) and calculated (Cal) pop-in data showing the load at the pop-in event versus the pop-in extension in (a) GaAs and InP and (b) GaN and ZnO.

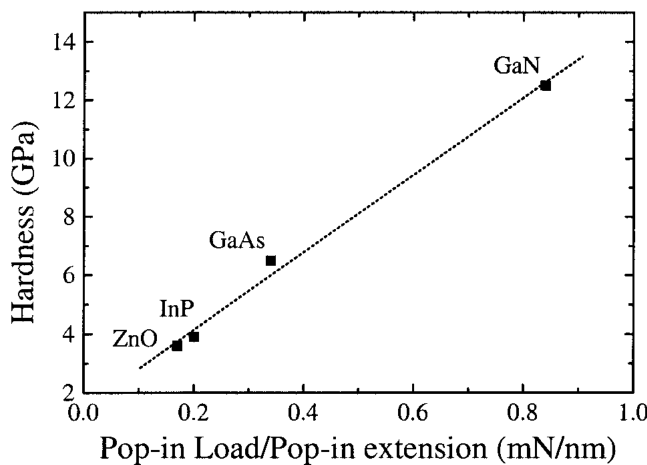

FIG. 3. Relationship between the hardness and the gradient of the calculated pop-in load versus extension curves shown in Fig. 2.

GaN, which has the highest hardness value of approximately 12.5 GPa. Indeed, from the analysis of Field and Swain[28] it can be shown that the rate of change of the load as a function of extension during pop-in should be broadly proportional to the hardness. [For spherical indentation, it follows from geometrical considerations that the pop-in depth is equal to the difference between the elastic-Eq. (1)-and plastic indenter displacement. From this it can further be shown that the change of depth with load is essentially proportional to the hardness, with only a weak dependency on the load.] Hence the gradient in the plots shown in Fig. 2 is directly related to the energy released upon the initiation of dislocations in these compound semiconductor materials and in turn scales with the hardness of the material. Specific features of each of the materials will now be discussed in terms of the mechanical behavior of the individual materials.

As can be seen in Fig. 2(a), the correlation between the calculated and experimental data corresponds well for InP. The measured pop-in load was found to vary between 10 and 18 mN with the corresponding pop-in extensions between approximately 30 and approximately 60 nm. From previous studies of spherical indents in InP it was found that cracking in this material was not observed up to a load of 25 mN (using a spherical indenter of ~4.2 μm).[10]

In contrast to InP, the calculated pop-in behavior for GaAs was not as successful in predicting the pop-in extensions across the range of measured pop-in loads. Indeed, as can be seen in Fig. 2(a), above approximately 38 mN the experimentally observed indenter extensions during the pop-in event are significantly smaller than is predicted from the calculated data. For example, at a load of 45 mN, the calculated data predicts a pop-in extension of approximately 82 nm while the experimental data shows a pop-in extension of only about 73 nm. One possible explanation for this difference is the previously reported observation that a crack forms in GaAs at loads approaching 50 mN.[10,31] This is clearly demonstrated in Fig. 4, which shows bright-field cross-sectional transmission electron microscopy (XTEM) images of indents made in GaAs at load of (a) 40 mN and (b) 50 mN. It can been seen that the main mode of deformation is slip along the {111} planes. At the orientation shown in Fig. 4, two of the {111} planes converge and intersect beneath the surface. A median crack, denoted as MC in Fig. 4(b), can be seen under the 50 mN indent. This crack appears to form at the intersection of the converging {111} slip bands and has previously been reported both in InP and GaAs.[10] Hence, the propensity of GaAs to crack at loads approaching 50 mN may account for the deviation of the experimental and calculated pop-in data at larger pop-in loads. At these higher loads, the measured indenter extension during the pop-in event may be reduced by the initiation of cracking and/or by work-hardening effects. Note that this behavior is not observed for InP, the other cubic material examined in this study. This may be due to the fact that cracking in InP has not been observed at the pop-in loads (10–18 mN) measured in this current study.

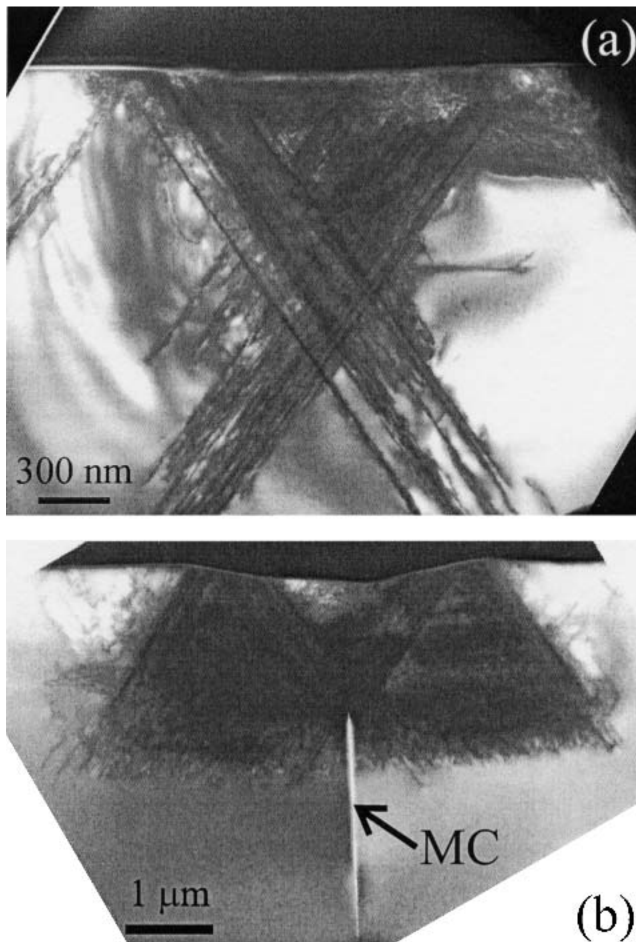

FIG. 4. Bright-field XTEM images showing indentation-induced damage in GaAs indented using a spherical indenter of ~4.2-μm radius to a maximum load of (a) 40 mN and (b) 50 mN. "MC" denotes the median crack. (Adapted from Ref. 10.)

We will now examine the pop-in results from the hexagonal materials ZnO and GaN, shown in Fig. 2(b). It has previously been reported that both GaN and ZnO exhibit multiple pop-in events during loading.[11,17] Note that for this current study, the experimental pop-in load and pop-in extension were measured only for the first pop-in event. From Fig. 2(b) it can be seen that the scatter in the experimental data is greater than that observed for the cubic materials. A possible explanation for this effect may arise from the nature of the mechanical deformation in these hexagonal materials. From our previous studies of indentation-induced deformation in GaN and ZnO, it was found that slip is initiated along two slip systems (both the basal and pyramidal planes).[11,17] As these two systems intersect, dislocations are impeded by the other slip system during plastic deformation. Unlike the scenario for the cubic materials discussed above, this intersection of slip systems in the hexagonal materials appears not to lead to crack formation. Specifically, we have observed no evidence for cracking in either GaN or ZnO at loads of up to 900 and 200 mN, respectively.[16,17] Instead, a profound pile-up of the material far from the indenter contact diameter was noted, suggesting that, as loading continues, further dislocations are punched out into the surrounding material. This nucleation and pile-up process (so-called slip stick behavior in Ref. 12) may account for the observed multiple pop-in events during a single loading cycle.[11,17] Indeed, XTEM images of indentation-induced deformation in ZnO reveals that slip along the basal planes may act as pinning sites for subsequent slip.[12] Thus, the interaction between the slip on the basal and pyramidal planes may influence the indenter extension during each individual pop-in event, causing the scatter in the experimental data observed in Fig. 2(b).

In addition to the effects outlined above, the indentation-induced deformation of GaN is further complicated by the presence of as-grown defects. Unlike the other three materials in this study, the GaN sample examined here is not a near-perfect bulk crystal, but instead consists of an approximately 2-μm epilayer grown on a sapphire substrate. Partly due to the lattice mismatch between GaN and sapphire (~16%), the resulting layer of GaN typically contains threading dislocations.[32] These defects form as the layer is grown and can be seen in the bright-field XTEM image shown in Fig. 5 (denoted by AG). This image also shows three bands of defects aligned along the basal planes induced by indentation loading with a spherical indenter. The interaction between the as-grown defects and the indentation-induced slip bands may add to the scatter in the experimental pop-in data shown in Fig. 2(b).

In contrast to GaN, pre-existing defects were not present in the bulk single-crystal ZnO samples examined in this study. Aside from the scatter in the experimental data discussed above, a reasonable correlation between the calculated and measured pop-in data is observed for ZnO

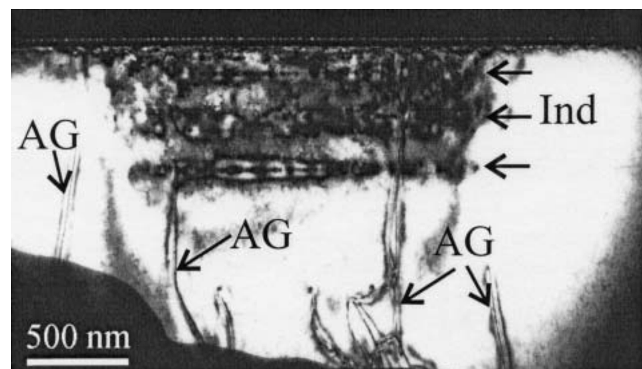

FIG. 5. Bright-field XTEM image showing indentation-induced damage in GaN loaded to 50 mN with a spherical indenter of ~4.2-μm radius. "AG" refers to as-grown dislocations and "Ind" the indentation-induced slip that is aligned along the basal planes. (Adapted from Ref. 11.)

[Fig. 2(b)]. It is interesting to note that the range of indenter extensions (~15–95 nm) is much greater for ZnO than any of the other materials in this study. This may be due to the previously observed ability of the indentation-induced dislocations in ZnO to extend far beyond the initial contact diameter of the indenter.[12] This may be more readily understood upon considering that the lower hardness value of ZnO results in a large diameter of indenter contact whereas in the elastic regime, the displacement is related to $E^{-2/3}$ [Eq. (1)].

It is interesting to reflect on the nature of the pop-in event in light of the above results. The elastic behavior of the materials at loads below the pop-in event indicates that no detectable plastic deformation is occurring before pop-in. Thus, the pop-in event in these materials appears to mark the initiation of dislocation motion that occurs upon the onset of plastic deformation. Indeed, we have found no evidence of slip or any plastic deformation in GaAs loaded below the pop-in event by XTEM or atomic force microscopy (AFM). Hence, although the pop-in event appears to mark the initiation of plastic flow, the range of the measured pop-in loads (23–45 mN for GaAs) were typically much greater than the calculated P_c value (~9 mN for GaAs). To further examine the yielding of the materials, the theoretical shear stress (τ_c) of each material was compared to the maximum shear, stress induced under the indenter τ_T prior to the pop-in event. This is shown in Table II. The theoretical shear stress was approximated to be a tenth of the shear modulus for each material (as suggested in a recent paper by Lorenz et al.[33]). The shear stress induced under the indenter was calculated using Eq. (6):

$$\tau_T = 0.465\, p_m \quad , \tag{6}$$

where p_m is the average contact pressure just prior to the pop-in event.[33] The range of τ_T reflects the range of loads at which the pop-in effect was observed to occur for each of the materials studied. The percentage of the theoretical shear strength to the induced shear is also presented in this table. This shows that the shear stress induced under the indenter (τ_T) immediately prior to the pop-in event approaches or exceeds the theoretical shear strength (τ_c) for GaAs, InP, and ZnO with a maximum percentage of τ_c of 107%, 97%, and 84%, respectively. However, for epitaxial GaN, the pop-in event occurs at shear stresses of 48–60% of τ_c. This suggests that the near complete absence of pre-exsisting dislocations in the GaAs, InP, and ZnO materials may lead to a higher "overload" pressure as a result of the need for a larger resultant subsurface shear stress to initiate slip. The epitaxial GaN layer, on the other hand, with the presence of as-grown threading dislocations, requires a far lower overload pressure to induce plasticity. This may indicate that the onset of plasticity in GaN may be triggered from exisiting dislocations that assist the nucleation of indentation-induced slip during loading.

TABLE II. The theoretical shear strength τ_c, the range of maximum shear strengths τ_T induced under the spherical indenter before the pop-in event, and the percentage of the theoretical shear strength achieved for the compound semiconductor materials studied.

Material	Theoretical shear strength (τ_c) (GPa)	Induced shear (τ_T) (GPa)	Percentage of τ_c achieved during indentation
GaAs	4.8	4.1–5.2	85–107%
InP	3.6	2.8–3.5	78–97%
ZnO	5.4	3.2–4.4	59–84%
GaN	15.7	7.6–9.4	48–60%

On this final point, it is interesting to consider a previous study by Kucheyev et al.[34] which compared the indentation behavior of GaN before and after ion implantation. The implantation treatment generated a high density of sessile defects. AFM imaging of the residual indent impressions both before and after implantation showed a dramatic suppression of the slip traces in the implanted sample as compared with the as-grown material. Similar behavior has also been observed by Nowak et al.[35] in ion-implanted sapphire and by Lorenz et al.[33] in CaF_2 after abrasive polishing. Thus, the presence of defects and the extent to which pre-existing dislocation loops are "pinned" prior to indentation may influence the load at which the initial pop-in event occurs but, as can be seen by the correlation between the experimental and calculated pop-in data [Fig. 2(b)], is not a strong influence on the subsequent extent of the pop-in event.

IV. CONCLUSIONS

We have demonstrated that it is possible to correlate the load at which a material undergoes pop-in with the resulting depth of indenter penetration. From elastic and elastic–plastic modeling we have shown that the pop-in event for the crystalline semiconductor materials examined in this study marks the transition from elastic to elastic–plastic behavior. Using these models, the indenter extension during the pop-in event was able to be predicted. Results from this study suggest that the presence of defects before indentation have a strong influence on the yielding behavior. This was observed in the epilayer-GaN sample that contained as-grown threading dislocations and yielded at relatively low-loads compared to the other near-perfect bulk materials studied.

ACKNOWLEDGMENTS

The authors would like to thank John Field for assistance with the modeling work presented in this paper and the referees for helpful comments.

REFERENCES

1. W.W. Gerberich, J.C. Nelson, E.T. Lilleodden, P. Anderson, and J.T. Wyrobek, Ann. Math. **44,** 3585 (1996).
2. S.A.S. Asif and J.B. Pethica, Philos. Mag. A **76,** 1105 (1997).
3. D.F. Bahr, D.E. Wilson, and D.A. Crowson, J. Mater. Res. **14,** 2269 (1999).
4. J.D. Kiely, K.F. Jarausch, J.E. Houston, and P.E. Russell, J. Mater. Res. **14,** 2219 (1999).
5. C. Tromas, J.C. Girard, V. Audurier, and J. Woirgard, J. Mater. Sci. **34,** 5337 (1999).
6. A. Gouldstone, H.J. Koh, K.Y. Zeng, A.E. Giannakopoulos, and S. Suresh, Acta Mater. **28,** 2277 (2000).
7. D.E. Kramer, K.B. Yoder, and W.W. Gerberich, Philos. Mag. A **81,** 2033 (2001).
8. T.F. Page, L. Riester, and S.V. Hainsworth, in *Fundamentals of Nanoindentation and Nanotribology,* edited by N.R. Moody, W.W. Gerberich, N. Burnham, and S.P. Baker (Mater. Res. Soc. Symp. Proc. **522,** Warrendale, PA, 1998), p. 113.
9. K.J.V. Vliet, J. Li, S. Yip, and S. Suresh, Phys. Rev. B **67,** 104105 (2003).
10. J.E. Bradby, J.S. Williams, J. Wong-Leung, M.V. Swain, and P. Munroe, Appl. Phys. Lett. **78,** 3235 (2001).
11. J.E. Bradby, S.O. Kucheyev, J.S. Williams, J. Wong-Leung, M.V. Swain, P. Munroe, G. Li, and M.R. Phillips, Appl. Phys. Lett. **80,** 383 (2002).
12. J.E. Bradby, S.O. Kucheyev, J.S. Williams, C. Jagadish, M.V. Swain, P. Munroe, and M.R. Phillips, Appl. Phys. Lett. **80,** 4537 (2002).
13. S.V. Hainsworth, A.J. Whithead, and T.F. Page, in *Plastic Deformation of Ceramics,* edited by R.C. Bradt, C.A. Brookes, and J.L. Routbort (Plenum Press, New York, 1995), pp. 173–184.
14. G. Yu, H. Ishikawa, T. Egawa, T. Soga, J. Watanabe, T. Jimbo, and M. Umeno, J. Cryst. Growth **189/190,** 701 (1998).
15. J.S. Williams, Y. Chen, J. Wong-Leung, A. Kerr, and M.V. Swain, J. Mater. Res. **14,** 2338 (1999).
16. S.O. Kucheyev, J.E. Bradby, J.S. Williams, C. Jagadish, M. Toth, M.R. Phillips, and M.V. Swain, Appl. Phys. Lett. **77,** 3373 (2000).
17. S.O. Kucheyev, J.E. Bradby, J.S. Williams, C. Jagadish, and M.V. Swain, Appl. Phys. Lett. **80,** 956 (2002).
18. E.L. Bourhis and G. Patriarche, Philos. Mag. Lett. **79,** 805 (1999).
19. G. Patriarche and E. LeBourhis, Philos. Mag. A **80,** 2899 (2000).
20. J.E. Bradby, J.S. Williams, J. Wong-Leung, M.V. Swain, and P. Munroe, Appl. Phys. Lett. **77,** 3749 (2000).
21. X.J. Ning, T. Perez, and P. Pirouz, Philos. Mag. A **72,** 837 (1995).
22. I. Yonenaga and T. Suzuki, Philos. Mag. Lett. **80,** 511 (2000).
23. L. Largeau, G. Patriarche, E.L. Bourhis, A. Rivière, and J.P. Rivière, Philos. Mag. **83,** 1653 (2003).
24. E.L. Bourhis, G. Patriarche, J.P. Riviere, and A. Zozime, Phys. Status Solidi A **161,** 415 (1997).
25. J.L. Weyher, M. Albrecht, T. Wosinski, G. Nowak, H.P. Strunk, and S. Porowski, Mater. Sci. Eng. B **80,** 318 (2001).
26. J. Malzbender, J. Eur. Ceran. Soc. **23,** 1355 (2003).
27. K.L. Johnson, *Contact Mechanics* (Cambridge University Press, Cambridge, 1985).
28. J.S. Field and M.V. Swain, J. Mater. Res. **8,** 297 (1993).
29. E.R. Weppelmann, J.S. Field, and M.V. Swain, J. Mater. Res. **8,** 830 (1993).
30. I.N. Sneddon, Int. J. Eng. Sci. **3,** 47 (1965).
31. J.E. Bradby, J.S. Williams, J. Wong-Leung, S.O. Kucheyev, M.V. Swain, and P. Munroe, Philos. Mag. Lett. **82,** 1931 (2002).
32. X.J. Ning, F.R. Chien, P. Pirouz, J.W. Yang, and M.A. Khan, J. Mater. Res. **11,** 580 (1996).
33. D. Lorenz, A. Zeckzer, U. Hilpert, P. Grau, H. Johansen, and H.S. Leipner, Phys. Rev. B **67,** 172101 (2003).
34. S.O. Kucheyev, J.E. Bradby, J.S. Williams, C. Jagadish, M.V. Swain, and G. Li, Appl. Phys. Lett. **78,** 156 (2001).
35. R. Nowak, C.L. Li, and M.V. Swain, Mater. Sci. Eng. A **253,** 167 (1999).